# Structural studies of the phase separation of amorphous $Fe_xGe_{100-x}$ alloys

Robert D. Lorentz* and Arthur Bienenstock
*Department of Applied Physics, Stanford University, Stanford, California 94305*

Timothy I. Morrison†
*Argonne National Laboratory, Argonne, Illinois 60439-4843*
(Received 10 September 1993)

Small-angle x-ray scattering and x-ray-absorption near-edge spectroscopy (XANES) experiments have been performed on amorphous $Fe_xGe_{100-x}$ alloys over the composition range $0 \le x \le 72$. The observed small-angle x-ray-scattering patterns were compared both with those calculated for a model assuming segregation of the alloys into particular phases and with scattering patterns calculated for voids in a homogeneous matrix. The x-ray-absorption near-edge-structure data were used to test for phase separation. No large-scale phase separation is observed in the semiconductor-metal transition region (15–25 at. % Fe), but fine-scale, kinetically limited phase separation or other types of composition fluctuations cannot be ruled out. The results also indicate that phase separation occurs for alloys with $37 \le x \le 72$, with data consistent with separation into amorphous $FeGe_2$ and $Fe_3Ge$. Thus, ferromagnetic moment formation occurs in the phase-separated region, with the transition composition (40–43 at. % Fe) probably linked to $a$-$Fe_3Ge$ percolation, as hypothesized by Janot for the related $Fe_xSn_{100-x}$ system. This phase separation explains the Mossbauer observation of "magnetic" and "nonmagnetic" Fe atoms in these alloys.

## I. INTRODUCTION

This paper deals with the determination of atomic arrangements in amorphous ($a$-) $Fe_xGe_{100-x}$ alloy films. Using vapor deposition, such films may be prepared over the broad composition range $0 \le x \le 72$, in which there are striking changes of physical properties. Pure $a$-Ge is a semiconductor with an open (low-density) structure. With the addition of Fe, it undergoes a semiconductor-to-metal transition which has been reported to occur at about $x = 25$ for evaporated films,[1] but which has recently been seen to occur at about $x = 15$ (Ref. 2) for the sputtered alloys used in this study. This change in electrical behavior may be due to the continuous decrease of the band gap to zero in homogeneous alloys or may be due to segregation of the alloys into distinct amorphous phases. A determination of whether the samples in this composition region are homogeneous or are, instead, phase separated is necessary in order to enable a better understanding of the mechanism for this transition.

The formation of moments on iron atoms in the $a$-$Fe_xGe_{100-x}$ system has been widely observed at a critical concentration $x_c$ of about 40 at. % Fe,[3] above which their values increase sharply. A recent determination using Mossbauer spectroscopy[4] on the same samples used in this study has found a critical iron concentration of about 43 at. % Fe. Other amorphous Fe-$M$ ($M$ = B,Si,Sn) systems show similar magnetic behavior, all with $x_c \approx 40$ at. % Fe, according to Mangin *et al.*[3] and Chien and Unruh.[5] Most explanations concerning this transition have implicitly assumed that these alloys are homogeneous. An exception to this is Janot's hypothesis[6] that $a$-$Fe_xSn_{100-x}$ alloys are phase separated into $a$-$FeSn_2$ and $Fe_3Sn$ in the composition region $33 < x < 75$. A determination of the atomic arrangements in the neighborhood of $x_c$ is helpful to understand the formation of these moments, and the possibility of phase separation in this region is thus important to address.

The question addressed in this paper is whether the amorphous films are chemically homogeneous. The crystalline Fe-Ge system contains several compounds, such as $FeGe_2$, FeGe (monoclinic, hexagonal, and cubic), $Fe_6Ge_5$, and $Fe_3Ge$ (hexagonal and cubic).[7] The equilibrium phase diagram consists of two-phase regions with essentially no regions of solid solubility. Thus, it would not be unreasonable for the metastable equilibrium amorphous states to be phase separated. Yet, there is often considerably more solubility in an amorphous phase than in the corresponding crystalline one, so that the question is truly open. With the exception of Janot's work, most explanations concerning the transition to moment formation have implicitly assumed that these alloys are homogeneous. It is important to determine whether that assumption is appropriate. In a second paper, studies of short-range order in these materials will be presented.

A structural study of amorphous Mo-Ge alloys (0–65 at. % Mo) by Kortright and Bienenstock[8] has addressed the possibility of phase separation in that system. No large-scale phase separation was detected for any composition. Fine-scale mixing of the random tetrahedral $a$-Ge network and Mo-modified material with short-range structure similar to that of the Ge-rich intermetallics is consistent with the structural results for the 0–23 % Mo samples. This region includes the semiconductor-metal transition. All indications of tetrahedral $a$-Ge disappear at about 23 at. % Mo. The region from about 23 to about

 

50 % Mo is characterized by strong ordering of Ge about Mo at short distances, long Mo-Mo first-neighbor distances, and a lack of preferred Ge-Ge distances. The collapse of the long Mo-Mo first-neighbor distances delimits this region from the more Mo-rich materials, which show structures typical of melt-quenched metal-metalloid glasses. One goal of this work was to determine whether the Fe-Ge system, whose equilibrium characteristics differ appreciably from those of Mo-Ge, shows different features in the amorphous films.

Two techniques have been used to approach the chemical homogeneity and/or phase-separation problem. Small-angle x-ray scattering (SAXS) is sensitive to long-range ($>10$ Å) electron-density fluctuations. These might arise from voids or other defects or from composition fluctuations. As a consequence, such measurements often yield ambiguous results concerning the presence of composition fluctuations. This ambiguity is discussed further below.

The second approach involves the examination of x-ray-absorption near-edge structure (XANES). This method is based on work comparing annealed *a*-Ge with a mixture of crystalline Ge and as-deposited *a*-Ge (Ref. 9) to test for phase mixing. If a sample was truly phase separated and a state close to metastable equilibrium was achieved, then one would anticipate that the XANES pattern would be a superposition of the XANES patterns from the two constituents. As a result, the XANES patterns from all samples in the two-phase region would be linearly dependent.

In considering these two approaches, one must keep in mind that the films studied in this paper were prepared by vapor deposition. As a result, they may not achieve even metastable equilibrium if that state involves phase separation. The vapor deposition process tends to yield homogeneous material. One might anticipate progress towards phase separation if the deposition is slow relative to surface mobility rates. Once the surface is covered over, however, the usually much slower bulk diffusion rates are the important ones. Thus, a sample might show composition fluctuations observable by SAXS, while not yielding the XANES linear dependence which would be gained if the sample had approached metastable equilibrium more completely.

The experimental and data analysis procedures are described below in Secs. II and III, respectively. The results are presented in Sec. IV and are discussed more fully in Sec. V. It is shown in Sec. V that the combination of the two techniques provides plausible explanations of a number of the observed magnetic phenomena in this system. In addition, a plausible explanation of the significant difference between the semiconductor-metal transition composition for sputtered and evaporated films is presented.

## II. EXPERIMENTAL PROCEDURES

### A. Sample preparation

All of the amorphous Fe-Ge samples used in this study were prepared as thin films by sputter co-deposition at Stanford University's Center for Materials Research Vapor Phase Synthesis Laboratory. Separate 2 in. targets of high-purity Fe and Ge were fixed to different cathodes in the vacuum chamber. By varying the deposition rates independently, samples of different compositions were prepared. The Ge target was used with a magnetron apparatus, while the Fe target was attached to a triode device. The sputtering guns were located at the bottom of the vacuum chamber, below the table holding the substrates, resulting in a sputter-up geometry. These targets were typically between 3 and 4.5 in. from the table, depending on the deposition rates and the composition desired. Since separate Fe and Ge targets were used, the table to which the substrates were held was rotated at 5 revolutions per second. The typical deposition rate was about 1.2 Å per second, corresponding to 0.24 Å/rev, which is much less than a monolayer per revolution. The alloys were deposited on 0.001 in. thick Kapton substrates and were between 0.14 and 2.7 $\mu$m thick.

The samples studied in these experiments had $x=0$, 5, 7, 12, 18, 20, 27, 30, 33, 37, 44, 45, 49, 65, and 72, as determined by Auger Microprobe. Several of the samples have been prepared with compositions similar to those of the crystal compounds occurring in the Fe-Ge system. The $x=33$ sample studied here has the same composition as the lowest iron concentration crystalline phase, *c*-$FeGe_2$, and the 72 at. % Fe alloy is close in composition to *c*-$Fe_3Ge$, the highest iron concentration compound in the system.

### B. Data collection

#### *1. Small-angle x-ray scattering*

The small-angle x-ray-scattering experiments were performed on the Beam Line 1-4 facility at the Stanford Sychrotron Radiation Laboratory (SSRL), which is described by Stephenson.[10] SAXS data were acquired for all amorphous samples except for $x=20$. The white radiation from the storage ring was monochromatized by a curved crystal and focused with a mirror. The amorphous Fe-Ge thin-film samples were stacked in order to achieve sufficient scattered intensity, which was measured by a photodiode array. Photomultiplier tubes with scintillation crystals placed before and after the sample to monitor the incident and transmitted intensities were used to normalize the scattering. The resulting measured $k$ range was $0.015<k<0.184$ Å$^{-1}$ using incident radiation of 8670 eV, where $k=(4\pi\sin\theta)/\lambda$. The optimum thickness for scattering in a transmission geometry for the stacked layers is given by $\mu t=1$. A value of $\mu t>0.3$ could be achieved for all but the thinnest samples. Being 25 $\mu$m thick, the Kapton substrate is many times thicker than each amorphous film and the substrate scattering cannot be neglected. Therefore, the contributions to the scattered intensity from the stacked Kapton substrate layers were measured to allow their subtraction. In the $k$ range of interest, the Kapton in-plane anisotropy observed by Boehme and Cargill[11] is small compared to other uncertainties and was neglected in this work. A dark current measurement performed with the beam off was

used to find the pixel response to background radiation and noise.

#### 2. *X-ray-absorption spectroscopy*

The x-ray-absorption near-edge structure data were obtained from x-ray-absorption experiments performed on all the amorphous samples. These data were collected on the unfocused bending magnet Beam Line 2-3 at SSRL where Si (220) crystals were used for monochromatization. The samples were placed in a cryostat and all scans were made with them near liquid-nitrogen temperature. Scans were made at both the Fe and Ge $K$ absorption edged from 1000 eV below the edges to 1200 eV above them. The double crystal monochromator was detuned 50% to reduce the harmonic content of the beam. The samples were stacked to achieve an increase in absorption at the edge, characterized by $\Delta\mu t$, of about 1.5 when possible. Ionization chambers filled with nitrogen gas, placed before and after the cryostat, were used to measure the incident and transmitted intensities. The same standard, an $a$-Ge thin film, was always used to calibrate the Ge $K$ absorption-edge energy, 11 103 eV, while $c$-Fe was used to calibrate the Fe edge data to 7112 eV. Several scans were made on each of the amorphous samples for later addition.

## III. DATA ANALYSIS

### A. SAXS

The SAXS data collected on the amorphous Fe-Ge samples, as well as on Kapton, were analyzed following procedures similar to those of Stephenson.[10] First, any bad pixels were eliminated from the data sets. The dark pattern was subtracted from both the Kapton and the total scattering data. Both the total and Kapton scattering were adjusted for the incident flux and the absorption using the photomultiplier-measured intensities. The average pixel efficiency (photodiode counts/photon) and the photomultiplier efficiencies determined by Stephenson[10] were used to put the data on an absolute scale. The Kapton substrate's scattering contribution was then subtracted from that of the sample. The resulting sample scattering data were then divided by the thickness of the stacked film. These procedures effectively divide the samples' scattering by $I_0 t \exp(-\mu t)$ to remove sample-size effects and to normalize the scattering to the incident flux, hence determining the scattering efficiency per unit thickness. The scattered efficiency is then on an absolute scale with units of inverse length. The pixel numbers were converted into $k$-space values using the sample to detector distance, energy, and pixel spacing. The finite sizes of the photodiode pixels are neglected in this analysis. The scattered intensity was measured in the range $0.015 \leq k \leq 0.184$ Å$^{-1}$. Since the energy of the incident radiation, 8670 eV, is above the $K$ absorption edge of iron (7112 eV), some fluorescent x rays were emitted by the sample and were detected by the photodiode array. The fluorescence, being emitted isotropically, should contribute equally to all pixels of the array if the slight differences in distance to the high- and low-$k$ pixels and the sample-size effects are neglected. This has been observed for fluorescence from Ni.[10]

There are several sources of error for this experiment and these may be significant. In order to put these data on an absolute scale, knowledge of the film thicknesses and the efficiencies of the photomultiplier tubes are needed. Kortright[12] has found that these efficiencies may vary by a factor of about 2 from the values used, while the sample thicknesses are known to within about 10%. Thus, an uncertainty of about a factor of 2 is introduced into the determination of the absolute scattering efficiencies. The relative SAXS efficiencies between samples should be accurate, however, and the shapes of the scattering patterns will not be affected. In addition, surface roughness or handling-induced cracks in the bulk of the films may cause an increase in the magnitude of small-angle scattering primarily in the low-$k$ region, but this has not been seen to cause any structure in the scattering patterns beyond a monotonic decrease with $k$.[13] The possible errors in the measured efficiencies should still allow us to decide which models for the larger than atomic scale structure of the samples are viable, since many of the models considered are typically found to be off in amplitude by many times. The shapes of the scattering data can also eliminate some models. Thus, some conclusions regarding phase separation can be drawn from these data, in spite of the possible errors.

### B. XANES

The XANES data were determined by finding the imaginary parts of the anomalous scattering factors (ASF's) for these alloys. An atom's scattering factor $f(k,E)$ changes rapidly in the vicinity of one of its absorption edges, where

$$f(k,E)=f_0(k)+f'(k,E)+if''(k,E)\ , \tag{1}$$

where $k=(4\pi\sin\theta)/\lambda$, $f_0$ is the atomic scattering factor at high energies, $E$ is the incident photon energy, and $f'$ and $f''$ are the anomalous scattering factors. Far from an absorption edge, Cromer-Liberman[14] (CL) free-atom calculations of the ASF's are generally regarded as sufficiently accurate, while near the edge chemical effects can cause significant deviations from these values. By determining $f''$ experimentally using the absorption data acquired on our samples, however, chemical effects are included.

Determining the imaginary part of the anomalous scattering factor entails putting the absorption data on an absolute scale, which allows quantitative comparisons to be made with the XANES from different samples. The $K$-edge absorption data collected for each sample were analyzed following procedures similar to those of Hoyt, de Fontaine, and Warburton.[15] For a given sample, the absorption data for different scans were averaged, after the dark currents were subtracted, to yield $\ln(\Sigma I_0/\Sigma I)$. The detector response function and the absorption from the other species were separated from the absorption due to the species of interest. To do this, a polynomial was fit to the pre-edge region of the data and the resulting function was subtracted from the entire data set, removing

the detector response function as well as the absorption from the lower shells and the other atom. Only the absorption due to the $K$ shell remained and these values were multiplied by $E$ in order to make these data proportional to $f''$ using the optical equation

$$f''(k=0,E)=\left[\frac{mc}{4\pi e^2 h}\right]\cdot E\cdot\sigma(k=0,E)\ . \tag{2}$$

A scale factor was determined by matching a point far above the edge, where chemical effects and extended x-ray-absorption fine-structure (EXAFS) oscillations are expected to be negligible, with a CL calculation of $f''$ for this energy. With this scale factor, the $f''$ values due to the $K$ shell of the atom were determined and the $f''$ contributions from the lower shells were then added using CL values.

## IV. RESULTS

### A. SAXS

Representative small-angle scattering patterns from some samples are shown on an offset scale in Fig. 1. For samples with $0\le x\le 33$, the scattering efficiencies fall off quickly and smoothly. From $37\le x\le 65$, the scattering efficiencies display significantly different behavior. In this range, either the rate of decrease with $k$ is much more gradual, with a shoulder sometimes present, or a well-resolved peak is present. At $x=72$, the steep decrease characteristic of the $0\le x\le 33$ range is again seen.

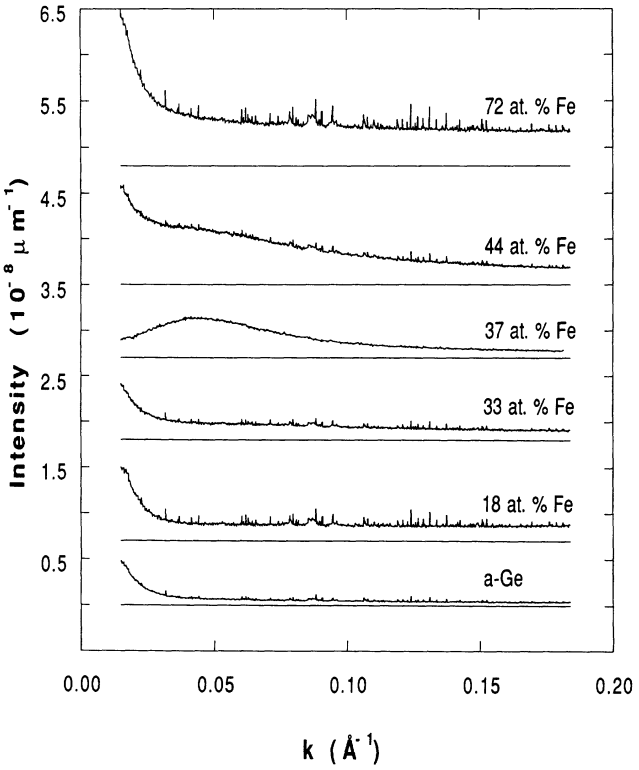


FIG. 1. Small-angle x-ray scattering patterns from several samples vs scattering vector magnitude $k$, shown on an offset scale.

#### 1. SAXS modeling procedures

SAXS can arise from many sources, including phase separation, voids, etc. To determine which of these are, and are not, consistent with the experimentally observed patterns, the scattering from several simple models was calculated. All modeling was done assuming spherically symmetric particles of a given radius in a homogeneous matrix. The scattered efficiency per unit sample thickness $I(kR)$ for closely packed spherical particles[16] as an approximate solution for a fluid of noninteracting hard spheres is given by

$$I(kR)=\left[\frac{e^2}{mx^2}\right]^2\rho_v(\rho_m-\rho_p)^2 \times V_0^2 d\Omega\left[\frac{\Phi^2(kR)}{1+(8V_0/V_1)\Phi(2kR)}\right], \tag{3}$$

where

$$\Phi(x)=3\left[\frac{\sin x - x\cos x}{x^3}\right], \tag{4}$$

$V_0$ is the volume of each sphere $=\frac{4}{3}\pi R^3$, $v_1$ is the volume offered to each particle $=\rho_v^{-1}$, $\rho_v$ is the density of particles by volume, $R$ is the radius of the spherical particle, $\rho_m$ is the matrix electron density, $\rho_p$ is the particle electron density, $d\Omega$ is the solid angle subtended by one pixel, and $k=(4\pi\sin\theta)/\lambda$, where $2\theta$ is the angle from sample to pixel. This function has units of inverse length. The calculated efficiencies are relatively insensitive to small variations in the choices of the electron densities for the matrix and particles used in the models. The idealized models are used here to determine whether phase separation or voids can account for the general shape and order of magnitude of the small-angle scattering intensities. We do not expect the models to be sufficiently sophisticated to yield detailed agreement with those intensities. The effects of pixel size and slit height have been neglected in this modeling and are not expected to be important on this scale.

#### 2. Comparison of models and experimental SAXS

Amorphous germanium is believed to consist of an amorphous matrix with voids in this matrix.[17] The resulting electron-density fluctuations give rise to small-angle scattering. By assuming a homogeneous Ge matrix with the $c$-Ge electron density and spherical voids, the low-$k$ part of the observed SAXS for $a$-Ge can be reproduced. A fit to the low-$k$ part of the $a$-Ge data using this model indicates that about 0.05% of the total volume is from voids with a radius of 106 Å. The high-$k$ scattering from the sample is significantly greater than that predicted by this model, however, but can be reproduced with an amorphous Ge matrix plus voids of about 10 Å, resulting in a density deficit of just under 6%. With a combination of these situations, the observed SAXS from a $a$-Ge can be reasonably reproduced (Fig. 2). This simple

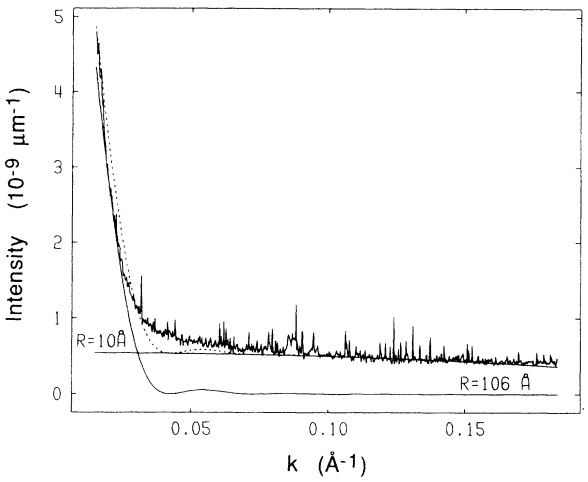


FIG. 2. SAXS from $a$-Ge, from a model with an amorphous Ge matrix plus voids of 106 Å, and from a model with 10-Å voids. The sum of the model scattering is plotted as a dotted line.

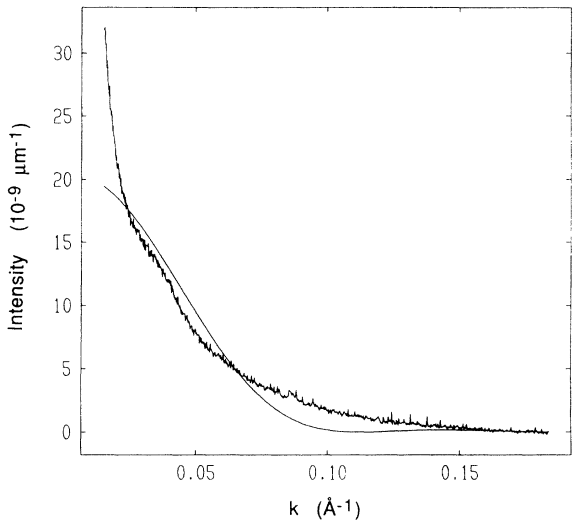


FIG. 3. SAXS from the 65 at.% Fe sample and from the model with an amorphous matrix plus voids of 40 Å in radius and density of $4.0\times10^{16}$ voids/cm$^3$.

model calculation is, then, consistent with the electron microscopy observations of interconnected microcracks about 6 Å in width and 120 Å in length by Donovan and co-workers[18,19] and the SAXS observations of small voids in sputtered $a$-Ge films by Shevchik and Paul.[20]

Modeling of the scattering from the other samples with SAXS patterns similar to that of $a$-Ge was attempted with a similar model having an amorphous $Fe_xGe_{100-x}$ matrix and spherical voids. The electron densities for these alloys were estimated by taking 95%, to account for lower densities in amorphous alloys, of the values obtained from a fit to the electron densities of the compounds in this system. Samples with $5\leq x\leq 33$ and $x=72$ can be reasonably well fit with this model, both at low $k$ and high $k$. All of these models are produced with about the same void radius and volume fraction of voids as in the $a$-Ge case.

For $37\leq x\leq 65$, however, the samples display very different small-angle scattering patterns. Some have broad, clearly resolved peaks, while others have slight shoulders on their very gradual decline to zero with increasing $k$. Those patterns with shoulders at low $k$ can be moderately well reproduced with this model, but with voids of about 40-Å radius and a density deficit of 1–5 % (Fig. 3). Those patterns having peaks at low $k$ cannot be fit by this model of an amorphous matrix plus voids, however; combinations producing peaks at the proper $k$ values have amplitudes between 30 and 130 times too large. Thus, $x=33$ seems to be a dividing point at and below which these samples' low-$k$ SAXS can be reasonably modeled by an amorphous matrix with voids of about 10 Å in radius, which comprise a few hundredths of a percent of the total volume. The SAXS from the 72% Fe sample can also be reasonably well fit by such a model.

To simplify the modeling of the prominent low-$k$ features of the SAXS data from each sample, such as steep slopes and broad peaks, the contributions to the observed scattering efficiency expected to be slowly varying over the $k$ range studied were removed by subtracting the sample's averaged high-$k$ scattering from the entire data set. This isolates the most significant SAXS signals and allows us to study their sources without having to simultaneously consider the background signals, such as fluorescence and scattering from small voids. Indeed, the presence of fluorescence signals makes it impossible for us to distinguish a model with small voids from a model with small second-phase regions. This is particularly important for samples with $x<33$, as is discussed below.

Simple models for large-scale phase separation using amorphous phases with the same electron and mass densities as those of several crystalline compounds have been investigated in an attempt to explain some features of the SAXS data from the alloys. In analogy with the equilibrium phase diagram for the Fe-Ge system, samples with $0<x<33$ may be expected to be separated into two amorphous phases similar to $c$-Ge and to $c$-$FeGe_2$. A model assuming a homogeneous $a$-Ge matrix and spherical particles of amorphous material, with the same electron and atomic densities as $c$-Ge and $c$-$FeGe_2$, respectively, was used to model the SAXS from these samples. When the particle radius was selected, the particle density was calculated to be consistent with the overall sample composition. When the particle radius was adjusted so that the model and experimental scattering efficiency curves had similar shapes, the intensities calculated from the models had magnitudes hundreds of times larger than those of the actual data. If a particle size was used which gave comparable scattering magnitudes at low $k$, the shape of the model curve was completely different from that of the experimental data; the model scattering was either flat across the entire $k$ range or the models produced a peak for any value of the radius, when the actual data display no peak. Models can also be constructed with these matrix and particle types interchanged. For this case, the matrix is now an amorphous phase with

densities similar to those of $c$-$FeGe_2$, with particles of $a$-Ge. Such models could not reproduce the observed SAXS data either.

The SAXS from the sample with $x=37$ has a maximum near $k=0.05$ Å$^{-1}$. Such a maximum cannot be produced by a low concentration of either voids or a second phase. Instead, there must be a relatively high concentration of voids or second phase, so that destructive interparticle interference leads to a decrease in the low-$k$ scattering, relative to the independent particle situation. We believe it extremely unlikely that such a high concentration of voids would be produced in these samples, since void formation and stability are much more likely in the more rigid $a$-Ge than at the metallic compositions. Hence, it is our belief that the maximum indicates the presence of phase separation.

For iron concentrations between 33% and 50%, the equilibrium state is a mixture of $c$-$FeGe_2$ and $c$-FeGe. Models with an amorphous matrix of the same electron and atomic densities as either $c$-$FeGe_2$ or $c$-FeGe and particles of the other amorphous phase were used to try to match the experimental SAXS in this composition range. The cubic phase of $c$-FeGe was used since the electron densities of $c$-$FeGe_2$ and monoclinic $c$-FeGe are equal and would produce no SAXS. The atomic and electron densities of the hexagonal polymorph of $c$-FeGe differ by only 13% from those of the cubic phase. The SAXS patterns for two of the samples in this range, $x=37$ and $x=44$, can be reasonably approximated by such models. No model could reproduce the smooth and gradual decrease with $k$ seen in the SAXS data for the $x=45$ sample, however, as any model producing reasonable scattering magnitudes always produced a well-resolved peak. In addition, the peak in the SAXS for $x=49$ could not be reproduced in amplitude and shape using these phases.

The samples whose SAXS patterns show significant scattering in the mid-$k$ range fall in the composition range $37 \le x \le 65$. This suggests that these samples may be separated into amorphous phases similar to $c$-$FeGe_2$ and to $c$-$Fe_3Ge$. Such a possibility was tested with a model using parameters from $c$-$FeGe_2$ and from the hexagonal phase of $c$-$Fe_3Ge$. The atomic and electron densities of the hexagonal and cubic polymorphs of $c$-$Fe_3Ge$ differ by less than 2%. These are six samples in the range from $FeGe_2$ to $Fe_3Ge$, two of which display well-resolved peaks in their SAXS patterns, while three others show a shoulder or a gradual decrease with $k$. The other, the 72% Fe alloy, shows only a sharp decrease at low $k$ and relatively little scattering at higher $k$. The SAXS observed for this sample may be well modeled with 12-Å particles of $FeGe_2$ in the $Fe_3Ge$ matrix. The corresponding particle density indicates that the $FeGe_2$ phase would make up about 8% of the sample by volume.

For the other alloys, the models' SAXS can reproduce the observed SAXS magnitudes from the samples to within a factor of 2, except for the $x=37$ sample where the model is too large by a factor of 5. For most of these samples, the models have reasonable amplitudes and in all cases, the general shape of the scattering can be reproduced moderately well. If there is a well-resolved peak in the observed scattering, a model can be generated with a peak at the proper $k$ value and an amplitude which is not too different, although the high $k$ falloff is usually too rapid. For the SAXS patterns which display shoulders, the main features can be reproduced reasonably well with these models, as indicated in Fig. 4. Since the sample will have a distribution of particle sizes and shapes, as opposed to the spherical particles of a single radius assumed here, these models can at best be reasonable approximations to the actual sample scattering. Given the uncertainty in absolute scale of the sample scattering, the fact that these models can reproduce the main features of the scattering indicates that segregation into amorphous phases similar to $c$-$FeGe_2$ and $c$-$Fe_3Ge$ is a possibility for samples in the range $37 \le x \le 72$.

Another possible mode of phase separation to be considered is segregation into $a$-Ge and an amorphous phase similar to $c$-$Fe_3Ge$. For this modeling of samples with $37 \le x \le 72$, the hexagonal phase of $c$-$Fe_3Ge$ was used. Of the six samples modeled with these phases, the best fits to the data from two are within a factor of 2 of the data, but the scattering from the other four cannot be fit with models that are better than 10 times too large. The ability of such models to explain the observed SAXS from this group of samples is thus doubtful.

The SAXS from the $x=65$ alloy has also been examined using a model with amorphous phases similar in

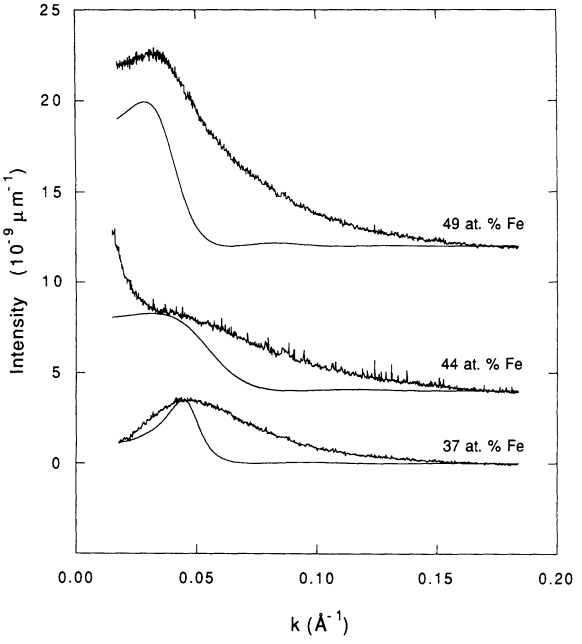


FIG. 4. SAXS from the 37, 44, and 49 at. % Fe alloys and models shown on an offset scale. The SAXS from the $x=37$ sample can be somewhat reproduced with 60-Å particles ($1.0\times10^{18}$ particles/cm$^3$) of $FeGe_2$ in an $Fe_3Ge$ matrix after the model is divided by 5. 50-Å particles ($4.3\times10^{17}$ particles/cm$^3$) of $Fe_3Ge$ in $FeGe_2$ reproduce the general shape of the scattering from the 44% sample after the model has been multiplied by 2. The model for the 49% Fe sample has 70-Å particles ($2.4\times10^{17}$ particles/cm$^3$) of $Fe_3Ge$ in $FeGe_2$.

atomic and electron densities to those of the monoclinic polymorph of *c*-FeGe and the hexagonal modification of *c*-$Fe_3Ge$. Although neither of the two combinations for the $x=65$ sample reproduces the observed sample scattering over the entire $k$ range, the position and amplitude of the shoulder seen in the SAXS data are reasonably well reproduced (Fig. 5). Since the observed SAXS is most likely a combination of scattering from a distribution of particles sizes, this model cannot be ruled out as a possible mode of phase separation for this sample. This mode would seem unlikely, however, since the amorphous sample close to *c*-FeGe in composition, $x=49$, itself appears to be of mixed phases. The SAXS from the 72% Fe alloy can also be well matched with this model.

The SAXS results can be summarized in the following way. For $x<33$, there is a scattering which falls off rapidly with increasing $k$, indicating relatively large ($>100$ Å) structure. We have not been successful in fitting this with a phase separation model and believe it likely that it arises from voids. In addition, there is SAXS which falls off very slowly. With the approach used here, we cannot tell if this arises from small voids or from composition inhomogeneities, because of Fe fluorescence. This problem is presently being addressed by Rice, Wakatsuki, and Bienenstock[21] using an anomalous SAXS approach similar to that of Goudeau *et al.*[22] A fine-scale ($<40$ Å) phase separation would be consistent with the conclusions of Kortright and Bienenstock[8] for the *a*-$Mo_xGe_{100-x}$ films with $x<33$.

For $33<x<72$, there appears to be true phase separation on a coarser scale ($>40$–$50$ Å) into regions similar to *c*-$FeGe_2$ and *c*-$Fe_3Ge$. We cannot, however, rule out the possibility that samples with $x=65$ and 72 are separated into regions similar to *c*-FeGe and *c*-$Fe_3Fe$.

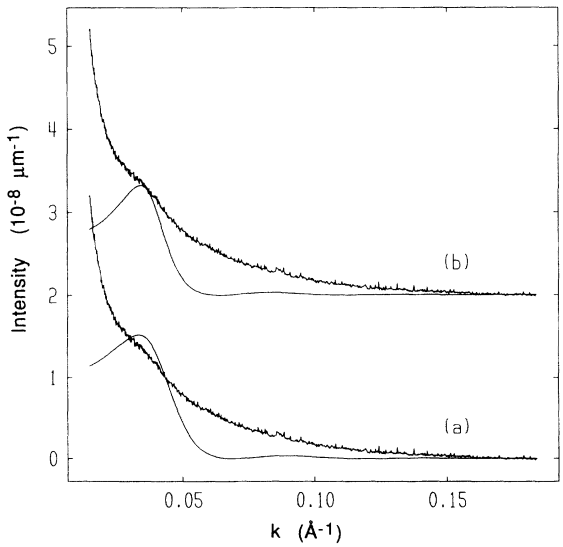


FIG. 5. SAXS for the 65 at. % Fe alloy and models shown on an offset scale. The model in (a) has 65-Å particles of FeGe ($4.0\times10^{17}$ particles/cm$^3$) in a $Fe_3Ge$ matrix, and is multiplied by 2. In (b), a model with 70-Å particles of $Fe_3Ge$ ($3.7\times10^{17}$ particles/cm$^3$) in FeGe reproduce the amplitude of the shoulder in the SAXS data from the sample.

## B. XANES

As stated in the Introduction, XANES can also be used to study phase separation in amorphous materials. If the phases in a mixed-phase sample are small enough and distributed so that the alloy appears homogeneous on the sample's size scale and if these phases are sufficiently large that the atoms at the phase boundaries contribute a negligible amount to the absorption, then the sample's absorption will be a linear combination of the absorptions of the constituent phases. Under such circumstances, the XANES from a phase-separated sample may be expressed as the weighted sum of the XANES from the individual phases. In an equilibrium phase diagram, the phases within a two-phase region are those which form the region's boundaries. Hence, the XANES from all samples within the region should be linearly related. In this section, analyses based on this concept are presented.

Only the Ge edge XANES from the samples were used in this test, since their features change significantly with composition. The changes are much less pronounced for the Fe-edge XANES. The large white line seen at the edge for *a*-Ge (Fig. 6) increases slowly in amplitude with iron concentration up to $x=37$, after which it falls sharply. Concurrent with the increase in white line amplitude is the narrowing of this peak. For $x\geq44$, the growth of a peak after the white line is observed. By 72% Fe, this second peak is larger in amplitude than the white line.

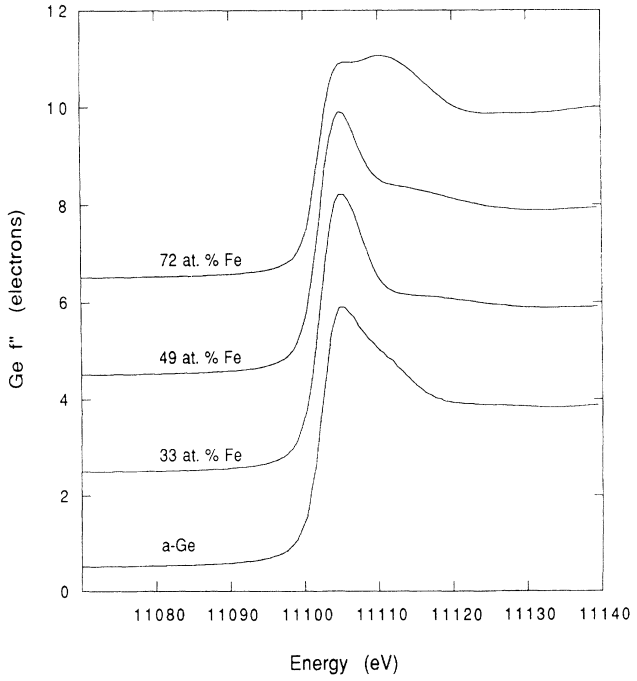


FIG. 6. Ge-edge XANES for *a*-Ge and $x=33$, 49, and 72 at. % Fe samples, shown on an offset scale. This series of spectra illustrates the strong effects that changes in the short-range order have on the XANES.

### 1. *XANES spectra analysis procedures*

The problem was formulated as follows to test whether the XANES spectra from sample $z$ can be expressed as a linear combination of the XANES from samples $x$ and $y$. Let spectra $\mathbf{z}$ be defined as

$$\mathbf{z}=a\mathbf{x}+b\mathbf{y} \tag{5}$$

where $a$ and $b$ are weighting coefficients and $\mathbf{z}$, $\mathbf{x}$, and $\mathbf{y}$ are vectors with $n$ components, each component being a point at which data were collected,

$$\mathbf{z}=\begin{bmatrix} z_1 \\ z_2 \\ \vdots \\ z_n \end{bmatrix}, \quad \mathbf{x}=\begin{bmatrix} x_1 \\ x_2 \\ \vdots \\ x_n \end{bmatrix}, \quad \mathbf{y}=\begin{bmatrix} y_1 \\ y_2 \\ \vdots \\ y_n \end{bmatrix}. \tag{6}$$

To test whether XANES spectra $\mathbf{z}$ is a linear combination of $\mathbf{x}$ and $\mathbf{y}$, we write

$$\mathbf{z}=\mathbf{M}\beta\ , \tag{7}$$

where

$$\mathbf{M}=\begin{bmatrix} x_1 & y_1 \\ x_2 & y_2 \\ \vdots & \vdots \\ x_n & y_n \end{bmatrix} \quad \text{and} \quad \beta=\begin{bmatrix} a \\ b \end{bmatrix}. \tag{8}$$

The solution $\beta$ to $\mathbf{z}=\mathbf{M}\beta$ is

$$\beta=(\mathbf{M}^{+}\mathbf{M})^{-1}\mathbf{M}^{+}\mathbf{z}\ , \tag{9}$$

where the $+$ indicates an adjoint. Given the three XANES data sets, the solutions $a$ and $b$ can be found easily and will give the best fit to Eq. (5) in the least-squares sense. If the fit to the test data set $\mathbf{z}$ is poor, or if either $a$ or $b$ are negative, which is unphysical, we can conclude that sample $z$ is not segregated into the same amorphous phases comprising $x$ and $y$. If the fit is reasonable with $a,b>0$, however, the samples $x$ and $y$ may represent the phases found in $z$. In this test, we have attempted both to find a region where the samples' XANES can be expressed as a linear combination of those from the other samples in this region as well as to find the end-point samples to such a region.

We can also test whether the coefficients $a$ and $b$ determine for each sample are reasonable. For a given sample with particular constituent phases $A$ and $B$ assumed, the expected coefficients can be calculated based on compositional arguments. Following Kunquan and Jun,[23] let $C_A$ and $W_A$ be the weight percent of the species whose absorption edge is being scanned in phase $A$ and the weight percent of phase $A$ in the sample, respectively. Then the absorption from the sample $\sigma_s$ will be a combination of the absorption from the individual phases

$$\sigma_s=C_A W_A \sigma_A+C_B W_B \sigma_B+\sigma_o\ , \tag{10}$$

where $\sigma_A$ and $\sigma_B$ are the $K$-shell contributions to the absorption and $\sigma_o$ is the absorption from the lower shells and the other atoms in the sample. The measured absorption $\sigma_{\text{meas}}$ will be proportional to $\sigma_s$,

$$\sigma_{\text{meas}}=\alpha(C_A W_A \sigma_A+C_B W_B \sigma_B+\sigma_o)\ . \tag{11}$$

The background absorption from the other atoms and the lower shells can be subtracted, leaving only the $K$-shell contribution to the absorption. Multiplying by a scale factor $\eta$ to match this to the $K$-shell contribution to $f''$ at an energy far above the edge where EXAFS oscillations and chemical effects are negligible, and using the optical equation gives

$$f''^{K}_{s}=\alpha\eta(C_A W_A f''^{K}_{A}+C_B W_B f''^{K}_{B})\ . \tag{12}$$

The $f''$ contributions from the other shells will add in the same way, so

$$f''_s=\alpha\eta(C_A W_A f''_A+C_B W_B f''_B)\ . \tag{13}$$

At energies far above the edge, the $f''$ values from each phase and the sample will be the same, so

$$\alpha\eta=(C_A W_A+C_B W_B)^{-1}\ . \tag{14}$$

Then

$$f''_s=af''_A+bf''_B\ , \tag{15}$$

where

$$a=\left[\frac{C_A W_A}{C_A W_A+C_B W_B}\right] \quad \text{and} \quad b=\left[\frac{C_B W_B}{C_A W_A+C_B W_B}\right]. \tag{16}$$

### 2. *Experimental spectra analysis*

Analysis of the XANES spectra shows that samples with $0\le x\le 33$ are not linear combinations of each other,

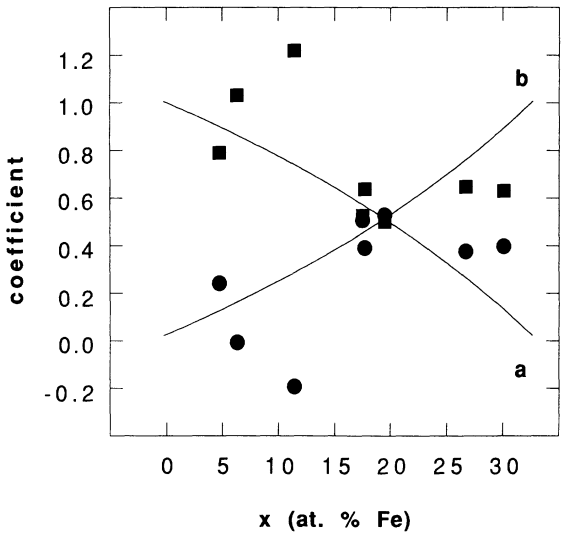


FIG. 7. Coefficients $a$ and $b$ of the XANES spectra for samples in the range $5\le x\le 30$. The lines are calculated using compositional arguments assuming separation of these samples into the phases $a$-Ge and $x=33$. The squares and circles represent the values of the coefficients $a$ and $b$, respectively, determined by fitting the XANES spectra from these samples with the spectra from the $a$-Ge and $x=33$ samples.

and that these spectra are not combinations of those from $a$-Ge and from any sample with $x \geq 33$. The values for the coefficients $a$ and $b$ calculated using compositional arguments, assuming separation of the samples in this range into $a$-Ge and $x = 33$ phases, are shown as lines in Fig. 7. Also shown are the experimentally determined values of $a$ and $b$ for our samples. The only composition for which the coefficients match well is $x = 20$. Here, the XANES spectra produced from the linear combination matches the experimental data reasonably well. For all other samples in this range, the experimentally determined values do not agree with the ones expected if the samples were separated into these phases and the fits between the generated and experimental data are poor. In Fig. 8, the XANES from the 12 at. % Fe sample and the least-squares fit using the $a$-Ge and $x = 33$ samples' XANES spectra are shown. For this sample, the coefficient of the $a$-Ge XANES is 1.22 and is $-0.22$ for the 33 at. % Fe sample's XANES. This fit is unphysical as well as poor. Based on compositional arguments, coefficients of 0.73 and 0.27, respectively, would be expected if the sample were indeed separated into these phases.

These tests have also shown that the XANES from samples in the range $37 \leq x \leq 65$ can be expressed as linear combinations of each other, however, and that all spectra from these samples can be described by a linear combination of the XANES from the 33% Fe and 72% Fe samples. For samples in this range, the coefficients expected if these samples are separated into the $x = 33$ and $x = 72$ phases are shown in Fig. 9 along with those values determined by fitting using the XANES spectra from these samples. In this case, the agreements are quite

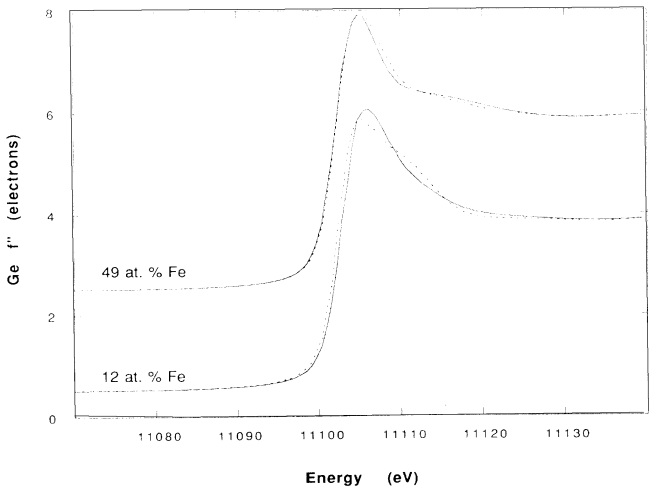


FIG. 8. (bottom) Ge-edge XANES from the 12 at. % Fe sample (solid) and the least-squares fit (dotted) using the XANES from the $a$-Ge and 33% Fe samples. The coefficients determined by fitting are 1.22 and $-0.22$, respectively, while those calculated from compositional arguments are 0.73 and 0.27. (top) Ge-edge XANES from the 49 at. % Fe sample (solid) and the least-squares fit (dotted) using the XANES from the 33% Fe and 72% Fe samples. The coefficients determined by fitting are 0.76 and 0.23, respectively, while those calculated from compositional arguments are 0.77 and 0.24.

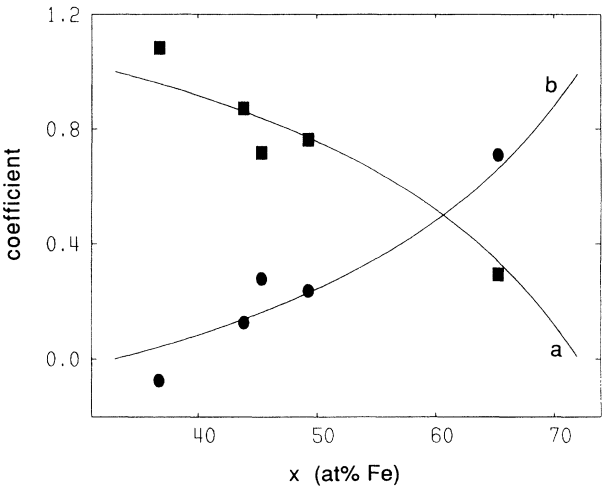


FIG. 9. Coefficients $a$ and $b$ of the XANES spectra for samples in the range $37 \leq x \leq 65$. The lines are calculated using compositional arguments assuming separation of these samples into the phases with $x = 33$ and $x = 72$. The squares and circles represent the values of the coefficients $a$ and $b$, respectively, determined by fitting the XANES spectra from these samples with the spectra from the $x = 33$ and $x = 72$ samples.

reasonable. The XANES from the $x = 49$ sample and the fit with the XANES from the $x = 33$ and $x = 72$ alloys are also shown in Fig. 8. The calculated coefficients for these phases are 0.77 and 0.24, respectively, and those determined by fitting are 0.76 and 0.23.

When the XANES from the $a$-Ge and 72% Fe samples are used as basis files, none of the other samples' spectra can be reasonably described; either the fits are poor or they are unphysical, with one component often being

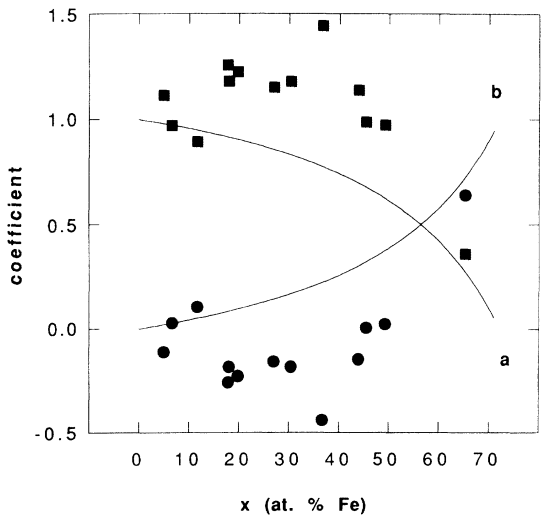


FIG. 10. Coefficients $a$ and $b$ of the XANES spectra for samples in the range $5 \leq x \leq 65$. The lines are calculated using compositional arguments assuming separation of these samples into the phases $a$-Ge and $x = 72$. The squares and circles represent the values of the coefficients $a$ and $b$, respectively, determined by fitting the XANES spectra from these samples with the spectra from the $a$-Ge and $x = 72$ samples.

significantly negative. The agreement between the coefficients calculated assuming separation of the samples into $a$-Ge and $x=72$ and the coefficients of the XANES spectra for these samples determined by fitting is quite poor (Fig. 10).

## V. DISCUSSION

The observations presented here may be summarized as follows: (1) For samples with $0 \leq x \leq 33$, the XANES imply that there is not large-scale phase separation into two metastable equilibrium amorphous phases. The SAXS patterns are consistent with either fine-scale chemical inhomogeneities or voids and similar defects, and are inconsistent with separation into $a$-Ge and $a$-$FeGe_2$.

(2) For samples with $33 \leq x \leq 72$, the XANES patterns are linearly dependent. The linear dependence is consistent with separation into the $x=33$ and $x=72$ samples. The SAXS patterns from samples with $37 \leq x \leq 65$ are quite different from those of the other samples. These show well-resolved peaks or broad declines with increasing $k$, as opposed to the rapid drops in the scattering at low-$k$ typical of samples in the range $0 \leq x \leq 33$ and for $x=72$. Such patterns cannot be reproduced by physically reasonable models involving an amorphous matrix and voids. The SAXS patterns may be modeled by a number of phase separation models, including separation into $x=33$ and $x=75$ phases.

As indicated above, the situation in the composition range $0 \leq x \leq 33$ is somewhat ambiguous, since we cannot distinguish between voids and fine-scale chemical inhomogeneities as the source of the SAXS, while the XANES results indicate that there is not a state which is well described as phase separation. Hence, the possibility exists that the metastable state of these amorphous materials is phase separation, but that the vapor deposition procedures followed in this work do not allow for that state to be reached. That is, the surface mobilities in this composition region are not high enough so that appreciable phase separation can be achieved before the outer layer is covered over.

If the equilibrium state is phase separation, then one would anticipate that the semiconductor-metal transition is a percolation transition. Since phase separation may be only partially achieved in the vapor description process, one would also anticipate that the details of the transition would depend markedly on sample preparation procedures and any subsequent heat treatment. A hint of this is contained in the large discrepancy between the transition composition measurements of Refs. 1 and 2.

If the metastable equilibrium state is phase separation in both regions, there is a significant difference between the phase separation kinetics for the $0 \leq x < 33$ and $x \geq 33$ regions. True separation appears to be achieved in the latter, but not in the former. A plausible explanation of this has been suggested by Turnbull.[24] He notes that surface diffusion rates tend to be considerably lower on semiconductor surfaces than on metallic surfaces. Under such circumstances, one would expect a considerably slower achievement of metastable equilibrium when most of the surface is semiconducting than when it is metallic. Such an argument would lead simply to a statement that one might expect the separation to proceed considerably more slowly for $x < 15$ (below the semiconductor-metal transition) than for $x > 33$, where all the surface is metallic.

The situation is more complicated for the region $15 < x < 33$, where the metallic state may be achieved through percolation. Since most of the surface diffusion would occur while the material was still homogeneous, further analysis requires knowledge of the composition at which the semiconductor-to-metal transition occurs for homogeneous material.

One hint is provided by the work of Daver, Massenet, and Chakraverty,[1] who reported a semiconductor-to-metal transition at between $x=20$ and $x=25$ for evaporated films. Since the energies of the impinging atoms are considerably lower in evaporation than in the sputtering used to produce the samples studied here, one would expect the evaporated film to be considerably closer to homogeneous. This argument would lead us to suspect that all the sputtered films with $x < 20$ will have insufficient time to phase separate appreciably, even if the metastable equilibrium is phase separated, because the homogeneous material is semiconducting, with relatively low surface diffusion rates. Since the samples with $x > 33$ do have time to phase separate, we would also expect samples with $x > 25$ to also have time.

The XANES fitting results shown in Fig. 7 are not, however, consistent with phase separation of the samples with $x > 25$ into $a$-Ge and $a$-$FeGe_2$. Thus, a model which is consistent with the data is one in which the metastable equilibrium structure of the samples with $x < 33$ involves microclustering of Fe atoms, but not phase separation. Such a situation has been suggested by Ding and Anderson[25] for Mo-Ge alloys in this composition range, based on molecular-dynamics studies. Their explanation for this could also apply to Fe-Ge alloys. Under such circumstances, the SAXS would show composition fluctuations, but the XANES would not necessarily indicate the linear dependence indicative of true phase separation.

We believe that the data for samples with $x < 33$ studied here are insufficient to truly distinguish between fine-scale segregation and homogeneity. If, however, the problem is kinetic (insufficient time to achieve phase separation), then it is possible that annealing studies will resolve the difficulty. Such studies will be pursued.

Based on the observations in point (2) above, we conclude that the films with $37 \leq x \leq 72$ are separated into two phases, which are likely to be $a$-$FeGe_2$ and $a$-$Fe_3Ge$. This composition region includes the magnetic transition which occurs at at $x=40-43$. The phase separation implies that the moment formation is associated with the presence of the $a$-$Fe_3Ge$ phase. Since this material is apparently present at $x=37$, one would anticipate moment formation if that formation is associated with short-range order. Thus, there is an apparent inconsistency.

It is interesting to note, however, that if one assumes that the densities of the $a$-$FeGe_2$ and $a$-$Fe_3Ge$ scale like the densities of the corresponding crystalline compounds, then the $a$-$Fe_3Ge$ phase would occupy 15 and 20 percent of the volume for the $x=40$ and $x=43$ compositions, re-

spectively. This implies that the composition range $x=40-43$ is precisely that in which percolation of the $a$-$Fe_3Ge$ phase would occur. Thus, it seems quite likely that the ferromagnetic moment formation is associated with percolation of $a$-$Fe_3Ge$. Since this transition is also seen in the related Fe-B, Fe-Si, and Fe-Sn systems, this is likely to be the origin of their transitions as well, as hypothesized by Janot.[6]

The fact that $c$-$FeGe_2$ is antiferromagnetic,[26] while $c$-$Fe_3Ge$ is ferromagnetic[27] lends support to this hypothesis. This hypothesis is also consistent with the observation from Mossbauer measurements on the alloys of Massenet *et al.*[28] that there are appreciable fractions of "nonmagnetic iron atoms" in the alloys with $x$ greater than 0.4. They state: "These nonmagnetic iron atoms correspond to more than 45% of the iron atoms present in the $Fe_{0.45}Ge_{0.55}$ alloy, and about 25% of those present in the $Fe_{0.55}Ge_{0.45}$ alloy." If the $a$-$FeGe_2$ contains the nonmagnetic iron atoms, then 53% and 29% of iron atoms would be nonmagnetic in the $x=0.45$ and $x=0.55$ samples, respectively. These numbers are in very good agreement with the observations of Massenet *et al.*[28]

Finally, one may anticipate significantly better characterization of the progress towards phase separation in amorphous films through the combination of the XANES procedures presented here and the anomalous small-angle scattering procedures of Goudeau *et al.*[22]

## ACKNOWLEDGMENTS

Special thanks are due to K. F. Ludwig, Jr. and S. Laderman for their valuable assistance. This research was performed at SSRL, which is operated by the Department of Energy, Office of Basic Energy Sciences, Division of Chemical Sciences. That Office's Division of Materials Sciences has provided support for the participation of A.B. and R.D.L. in this research.

*Present address: Storage Media Laboratory, 201-1E-17 3M Center, St. Paul, MN 55144.

†Present address: Department of Physics, Illinois Institute of Technology, Chicago, IL 60616.

[1]H. Daver, O. Massenet, and B. Chakraverty, in *Proceedings of the 5th International Conference on Amorphous and Liquid Semiconductors, Garmisch-Partenkirchen, 1973,* edited by J. Stuke and W. Brenig (Taylor & Francis, London, 1974), p. 1053.

[2]C. L. Tsai (private communication).

[3]P. Mangin, M. Piecuch, G. Marchal, and C. Janot, J. Phys. F **8**, 2085 (1978).

[4]N. S. Dixon and L. S. Fritz (private communication).

[5]C. L. Chien and K. M. Unruh, Phys. Rev. B **25**, 579 (1982).

[6]C. Janot, J. Non-Cryst. Solids **56**, 267 (1983).

[7]M. Richardson, Acta Chem. Scand. **21**, 2305 (1967).

[8]J. B. Kortright and A. Bienenstock, Phys. Rev. B **37**, 2979 (1988).

[9]T. I. Morrison, M. A. Paesler, D. E. Sayers, R. Tsu, and J. Gonzalez-Hernandez, Phys. Rev. B **31**, 5474 (1985).

[10]G. B. Stephenson, Ph.D. thesis, Stanford University, 1982 (unpublished); see, also, G. B. Stephenson, W. K. Warburton, W. Haller, and A. Bienenstock, Phys. Rev. B **43**, 13 417 (1991).

[11]R. F. Boehme and G. S. Cargill III, in *Polyimides,* edited by K. L. Mittal (Plenum, New York, 1984), Vol. 1, p. 461.

[12]J. B. Kortright (private communication).

[13]B. Rodmacq, P. Mangin, and A. Chamberod, Phys. Rev. B **30**, 6188 (1984).

[14]D. T. Cromer and D. Liberman, J. Chem. Phys. **53**, 1891 (1970).

[15]J. J. Hoyt, D. deFontaine, and W. K. Warburton, J. Appl. Cryst. **17**, 344 (1984).

[16]A. Guinier and G. Fournet, *Small-Angle Scattering of X Rays* (Wiley, New York, 1955).

[17]N. J. Shevchik and W. Paul, J. Non-Cryst. Solids **16**, 55 (1974).

[18]T. M. Donovan, W. E. Spicer, J. M. Bennett, and E. J. Ashley, Phys. Rev. B **2**, 397 (1970).

[19]T. M. Donovan and K. Heinemann, Phys. Rev. Lett. **27**, 1794 (1971).

[20]N. J. Shevchik and W. Paul, J. Non-Cryst. Solids **8-10**, 381 (1972).

[21]M. Rice, S. Wakatsuki, and A. Bienenstock, in *Thin Film Structures and Phase Stability,* MRS Symposia Proceedings No. 187 (Materials Research Society, Pittsburgh, 1990), p. 53.

[22]R. Goudeau, A. Naudon, A. Chamerod, B. Rodmacq, and C. W. Williams, Europhys. Lett. **3**, 269 (1987).

[23]L. Kunquan and W. Jun, Phys. Rev. B **35**, 4497 (1987).

[24]D. Turnbull (private communication).

[25]K. Ding and H. C. Anderson, Phys. Rev. B **34**, 6987 (1986).

[26]L. M. Corliss, J. M. Hastings, W. Kunnmann, R. Thomas, J. Zhuang, R. Butera, and D. Mukamel, Phys. Rev. B **31**, 4337 (1985).

[27]J. W. Drijver, S. G. Sinnema, and F. v. d. Woude, J. Phys. F **6**, 2165 (1976).

[28]O. Massenet, H. Daver, V. D. Nguyen, and J. P. Rebouillat, J. Phys. F **9**, 1687 (1979).